cigre Turkey

TEPES
TURKISH JOURNAL OF ELECTRICAL POWER AND ENERGY SYSTEMS

TEPES, Vol. 5, Issue. 2, 132-141, 2025 **DOI:** 10.5152/tepes.2025.24035

RESEARCH ARTICLE

Magnetic Sensor-Based Approach for Overhead Transmission Lines Fault Detection and Location Using Line Fault Current

Patrick Nyaaba Ayambire

Department of Electrical and Electronics Engineering, Akenten Appiah-Menka University of Skills Training and Entrepreneurial Development (AAMUSTED), Kumasi, Ghana

Cite this article as: P. N. Ayambire, "Magnetic sensor-based approach for overhead transmission lines fault detection and location using line fault current," *Turk J Electr Power Energy Syst.*, 2025; 5(2), 132-141.

ABSTRACT

This paper proposes a magnetic sensor-based approach to overhead transmission line fault detection and location. The proposed approach utilizes magnetic flux density measurements obtained using an array of magnetic sensors installed at the ends of a transmission line to measure currenttraveling waves. These measurements are analyzed to detect and locate faults. The scheme was implemented and tested using a transmission line modeled in Electrical Transient Analyzer Program and MATLAB/Simulink. The experimental evaluation validates the high efficiency of the scheme in measuring current traveling waves and accurately detecting and locating faults. Comparative analysis with a generalized traveling wave-based approach highlighted the validity and efficiency of the proposed approach. Across all test scenarios, the method delivered exceptional results, achieving an average percentage error of only 0.02445% in fault locations for various fault types.

Index Terms—Current traveling wave fault location, differentiator smoother, magnetic sensors, overhead transmission lines

I. INTRODUCTION

Overhead transmission lines are the most essential part of the modern power grid; however, these lines travel through several kilometers of rough forest terrain, making their operational management complicated. These important infrastructural assets are prone to a wide range of faults, such as conductor breaks, insulator failures, and tree and lightning strikes [1, 2].

The reliable operation of power transmission systems is critical for the efficient and effective transmission of electrical power across geographical areas, ensuring uninterrupted service to industrial, commercial, and residential users. An overhead transmission line is a major backbone for power transmission, but these lines are exposed to harsh environmental conditions, making them prone to various types of faults. Some of the faults, such as the various types of short circuit faults, grounding faults, and line breakages, can lead to disruptions in power supply, equipment damage, and financial losses.

Restoring service through accurate and reliable fault location approaches helps reduce outage duration, which brings about economic and societal consequences. Therefore, the development of efficient transmission line fault detection and location schemes is essential to maintaining the reliability and stability of the power supply.

These lines frequently break down because of the environment in which they are deployed [3], the lines mostly encounter frequent breakdowns. Nevertheless, these transmission lines are crucial for power supply, and the slightest disturbances may lead to power interruptions [4].

Detecting and locating faults is frequently one of the biggest obstacles to overhead power line monitoring. Since overhead transmission lines span a wide geographical area, it is challenging to pinpoint the fault spot for a prompt response. For this reason, a reliable plan that can record the occurrence in real-time is required.

Current transformers (CTs) and coupling capacitor voltage transformers are conventional tools for monitoring overhead power lines. These devices may, however, have certain operational limitations

Corresponding author: Patrick Nyaaba Ayambire, **E-mail:** pnayambire@aamusted.edu.gh

Received: November 25, 2024
Revision Requested: January 5, 2025
Last Revision Received: January 20, 2025
Accepted: January 31, 2025
Publication Date: March 25, 2025

when power lines encounter faults. Bindi et al. and Honcharov et al. [5, 6] proposed a scheme where CTs are placed on overhead power lines as part of a plan for current monitoring. It is important to note that because of their size, weight, and cost, CTs cannot be mounted outside substations for line monitoring.

Magnetic field sensors provide a fantastic possibility to achieve real-time power line monitoring, which offers a unique way to monitor overhead power lines. The importance of sensor-based monitoring of overhead power line parameters has been demonstrated by researchers throughout these years [7, 8].

Fault detection and location are essential for maintaining system dependability in transmission networks. To find a fault point in a long power line [9], proposed a scheme that uses magnetic sensors. However, the number of sensors utilized was not disclosed in the study, which could have impacted the scheme's accuracy.

Electric current parameters play a crucial role in power line monitoring. A strong continuous monitoring system that records system events in real time is required to guarantee reliable power delivery [10].

A sufficient measurement of the current traveling waves is necessary to establish useful findings when using current traveling waves to locate a power line fault. In this context, Abd et al. [11] proposed a lightning current measurement method for power lines that involves installing sensors on the lines. Despite being creative and innovative, the proposed scheme only addresses lightning issues.

For the utility and the customer, prompt and precise fault detection and location are critical during a power line failure [12, 13]. Line maintenance engineers need a precise fault distance as a reference to locate the fault point in the shortest amount of time. This will guarantee a faster system recovery and less income loss.

Researchers have proposed many fault detection and location schemes in the last 10 years. These schemes fall into two primary categories: the traveling wave-based scheme and the impedance-based scheme [14, 15].

Many power facilities use the impedance-based scheme because it is thought to be simpler, less costly, and less computational [16–18].

Main Points

- Overhead line fault detection and location using magnetic field sensors.
- The magnetic sensor array was used to measure the current traveling wave generated for fault detection.
- A mathematical scheme was formulated based on the sensor and conductor configuration.
- The study underscores the importance of magnetic sensors in achieving non-contact measurements.
- The study concluded with a comparative analysis of a proposed scheme published in the literature and the non-contact scheme proposed in this paper.

However, fault resistance, load flow, remote terminal data, and non-homogeneous systems all have an impact on the measurement accuracy of this scheme [19].

The traveling wave-based fault location technique was presented to address the drawbacks of the impedance-based fault location scheme [20–23]. When a fault occurs in a power line, traveling waves of high voltage and current are produced and travel in both directions along the line [24]. These traveling waves contain useful information that can be analyzed for the detection and location of faults. The traveling wave-based method relies on time synchronization and data-collecting systems [25].

Nevertheless, the method's reliability is diminished by the difficulty in identifying traveling waves that propagate from the fault point and those that are reflected from the fault point under various bus configurations [26–28]. Although these conventional fault detection and location schemes are proven schemes used by many entities across the globe, these schemes require major infrastructural investments, complex computational models, and are limited in terms of precision in remote or inaccessible areas. Furthermore, this approach requires rigorous time synchronization, which may lead to significant real-time fault distance estimation inaccuracies.

Due to the above-mentioned challenges highlighted in the literature reviewed in this study, the main contribution of this paper is to propose an efficient and cost-effective non-contact fault detection and location scheme for overhead transmission lines using magnetic sensors. The use of magnetic sensors for measuring current traveling waves in overhead transmission lines in this study is inspired by the research done in [8].

The proposed scheme presented in this study offers numerous advantages over the impedance-based scheme and the traveling wave-based scheme. Magnetic sensors are compact, cost-effective, require minimal maintenance, and can withstand harsh weather conditions. In this proposed scheme, the sensor arrays are installed at both towers of the transmission line. This will reduce the dependency on centralized infrastructure. Furthermore, the non-contact nature of magnetic sensors eliminates the need for direct electrical connections, enhancing safety, stability, and reliability.

This proposed approach to fault detection and location in overhead transmission lines provides a viable and transformative solution for overhead transmission line monitoring. The proposed technique takes advantage of magnetic sensors' ability to correctly monitor fault-induced fluctuations in line currents, allowing for precise fault identification and localization. In real-world applications, the approach can be realized by strategically installing small, cost-effective sensors along vantage points of the transmission line. The system is set to work independently by sending real-time data to control centers for immediate analysis and decision-making.

II. METHODOLOGY

A. General Principles of the Traveling Wave

When there is a fault on a power line, traveling waves are created and move in both directions of the line. These waves are the features

that a power line experiences when a fault causes a significant fluctuation in voltage and current. These traveling waves move at the speed of light towards the line's endpoints. The traveling waves contain vital information for fault detection and location. Using current and voltage traveling waves and the parameters of the line, and assuming a lossless line with minimal resistance and conductance, a mathematical relationship is established as shown in (1).

$$\begin{cases} -\dfrac{\partial v(x,t)}{\partial x} = L\dfrac{\partial i(x,t)}{\partial t} \\ -\dfrac{\partial i(x,t)}{\partial x} = C\dfrac{\partial v(x,t)}{\partial t} \end{cases} \quad (1)$$

As illustrated in Fig. 1, in a fault situation, current traveling waves are created and move toward the ends of the line. These waves are made up of both incident and reflected current traveling waves. The mathematical representation of the current traveling waves is expressed in (2):

$$I(t) = I_i(t) + I_r(t) \quad (2)$$

where I is the traveling wave, I_i and I_r are the incident and reflected traveling waves, respectively.

Fig. 2 gives an illustration of a non-contact schematic for measuring current traveling waves during a fault in an overhead transmission line. The schematic is equipped with a sensor array installed at each end of the transmission line. The sensor array installed at the end of the line, named as tower T_A and TB, records the current traveling waves as in (3):

$$I_A(t) = I_{ia}(t) + I_{ra}(t) \text{ and } I_B(t) = I_{ib}(t) + I_{rb}(t) \quad (3)$$

The data recorded consist of the incident and reflected current traveling waves as expressed in (4):

$$I_p(t) = \left(I_A(t) + I_B(t)\right)\sin\left(\omega(t) + \phi\right) \quad (4)$$

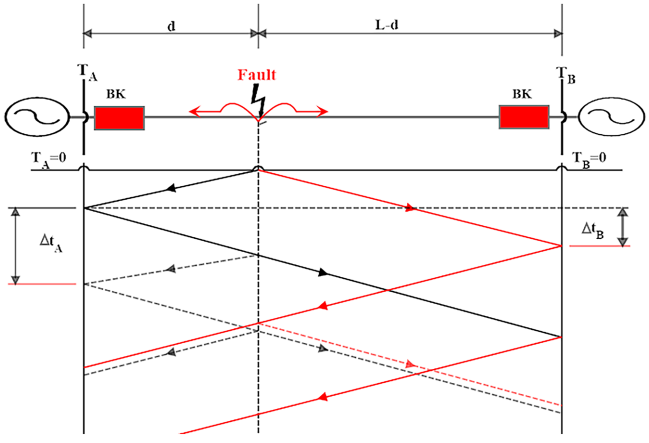

Fig. 1. Determining the arrival time of traveling wave faults for transmission lines.

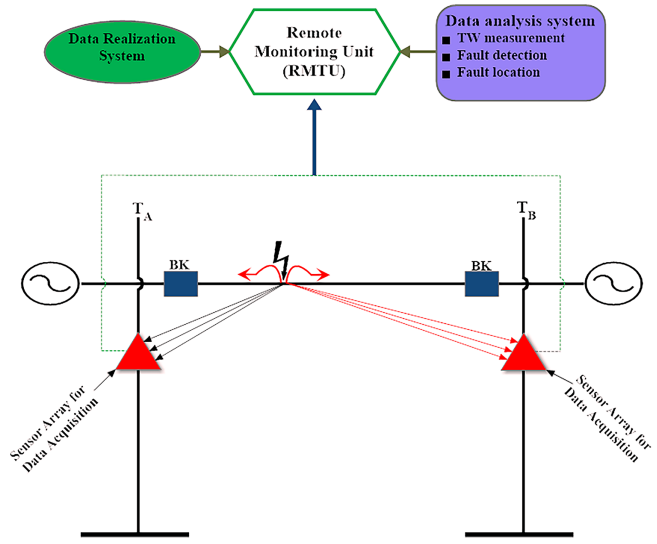

Fig. 2. Traveling wave fault location scheme.

where ω is the frequency, ϕ is the phase angle, and $I_p(t)$ is the peak at time t. If $(t) = 0$ is the fault current under typical operating conditions. However, (4) becomes $I_p(t) < I_f(t)$ in the case of a line fault. The data recorded by the sensor array are further analyzed for transmission line fault detection and location as explained in the proceeding section of this study.

B. Magnetic Sensor Based Measurement of Current Traveling Waves

A non-contact traveling waves fault location system is shown in Fig. 2. Sensor arrays are ideally positioned at both line towers in areas where maximum signals can be detected.

C. Mathematical Model of the Proposed Scheme

Overhead transmission lines are exposed to very bad weather conditions, so systems that are meant to monitor these lines must be robust and able to withstand harsh environmental conditions. The sensors used in this study can withstand temperatures ranging from −40°C to about 200°C and can function for up to 30 min at 250°C [8]. These magnetic sensors can operate successfully in adverse weather conditions. This allows them to be used for transmission line monitoring.

In this study, a monoaxial magnetic sensor was used to form the array. The array is installed at each end of the transmission line for the measurement of the magnetic flux density generated by the current traveling waves.

Fig. 3 illustrates a detailed cross-section of Fig. 2; it is a sensor array with three-phase conductors. The sensor array is made up of three magnetic sensors installed on the towers and three conductors configured in a triangular form. The currents passing through each conductor originate from a common supply and are measured at a distance greater than the diameter of the conductor. The placement of the sensors for the flux density computation is displayed in Fig. 4.

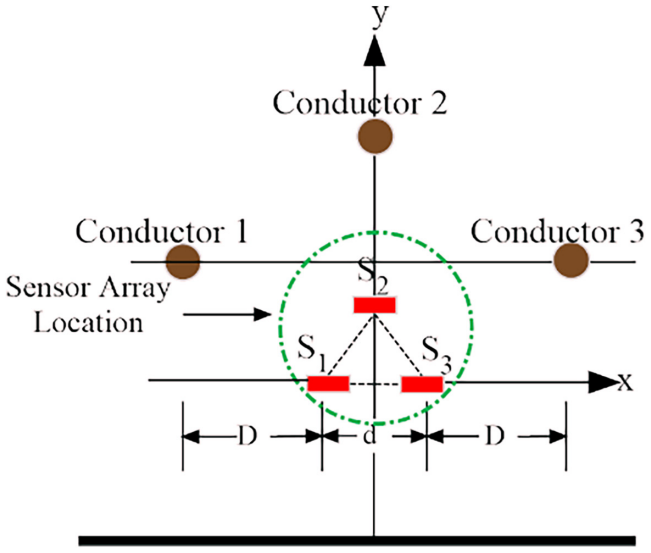

Fig. 3. Geometrical arrangement of conductor's configuration.

Based on the Biot–Savart law, the resultant flux density can be estimated. Ignoring conductors sagging and assuming that power lines are long when compared to the distance between the conductors and the point of measurement. A conductor in an x, y, and z plane produces the magnetic field shown in [9] as (5):

$$d\vec{B}_i = \frac{\mu_o I_i d\vec{l}_i \times \vec{r}}{4\pi r^3} \tag{5}$$

where $\vec{r} = (x - x_i)\check{i} + (y - y_i)\check{i} + 0\check{\kappa}$, $\mu_0 = 4\pi \times 10^{-7} N/A^2$ and $d\vec{l} = dz\check{k}$ are in the same as i_i and (5) is obtained from (4).

$$B_i = \frac{\mu_o I_i}{2\pi r_i} \tag{6}$$

When compared to a working power line that has no fault, the magnetic fields created by the fault current traveling waves are high in magnitude. Using (5) and ignoring conductor sagging, the magnetic

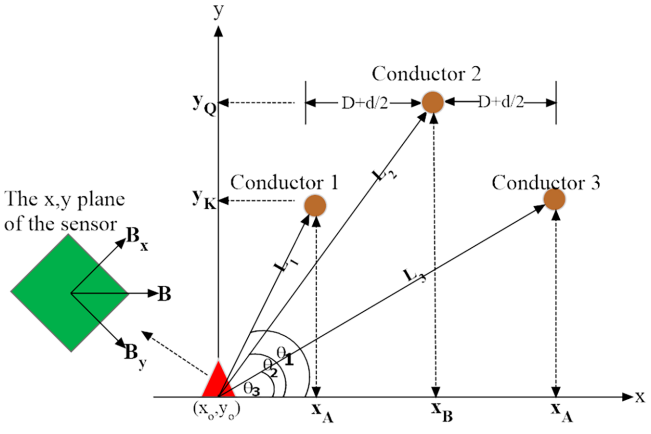

Fig. 4. Illustration of magnetic field at each sensor head location with current flowing along the z-axis.

flux BS_1, BS_2, and BS_3 produced by the current traveling waves as established in (4) from the individual conductors I_1, I_2, I_3 as I_{f1}, I_{f2}, and I_{f3} is expressed as (7):

$$B_j(x,t) = \frac{\mu_0 i_f(t)\sin(\omega t + \phi)}{\pi L_j}\left((y_0 - y_1) + (x_0 - x_1)\right) \tag{7}$$

where $L_i = \sqrt{(y_0 - y_1)^2 + (x_0 - x_1)^2}$ and $\left(I_A(t) + I_B(t)\right)\sin\left(\omega(t) + \phi\right) = I_f(t)$.

The magnetic flux created by the various conductors and measured by the sensor array located at optimal positions on the tower is determined using (8):

$$B_j(x,t) = \frac{\mu_0 I_{fj}(t)}{\pi L_j}\left((y_0 - y_i) + (x_0 - x_i)\right) \tag{8}$$

Current traveling waves of varying magnitude flow through these three conductors I_1, I_2, and I_3 during a transmission line fault. The x and y components of the magnetic flux sensed by the array are given in (9).

$$\begin{cases} B_{S11}(x,t) = \dfrac{\mu_0 I_{f1}(t)}{\pi L_{11}}\left((y_0 - y_K)\sin\theta_{11} + (x_0 - x_A)\cos\theta_{11}\right) \\ B_{S12}(x,t) = \dfrac{\mu_0 I_{f2}(t)}{\pi L_{12}}\left((y_0 - y_Q)\sin\theta_{12} + (x_0 - x_A)\cos\theta_{12}\right) \\ B_{S13}(x,t) = \dfrac{\mu_0 I_{f3}(t)}{\pi L_{13}}\left((y_0 - y_K)\sin\theta_{13} + (x_0 - x_A)\cos\theta_{13}\right) \end{cases} \tag{8}$$

The magnetic flux B_{S1} (x, t) detected by sensor S_1 is calculated using (10).

$$B_{S1}(t) = \sqrt{(B_{S11})^2 + (B_{S12})^2 + (B_{S13})^2} \tag{10}$$

Again, the magnetic flux produced by the conductors and detected by the sensor S_2 is computed as (11).

$$\begin{cases} B_{S21}(x,t) = \dfrac{\mu_0 I_{f1}(t)}{\pi L_{21}}\left((h - y_K)\sin\theta_{11} + (x_0 - x_A)\cos\theta_{21}\right) \\ B_{S22}(x,t) = \dfrac{\mu_0 I_{f2}(t)}{\pi L_{22}}\left((h - y_Q)\sin\theta_{12} + (x_0 - x_A)\cos\theta_{22}\right) \\ B_{S23}(x,t) = \dfrac{\mu_0 I_{f3}(t)}{\pi L_{23}}\left((h - y_K)\sin\theta_{23} + (x_0 - x_A)\cos\theta_{23}\right) \end{cases} \tag{11}$$

The magnetic flux B_{S2} (x, t) detected by sensor S_2 is computed using (12).

$$B_{S2}(t) = \sqrt{(B_{S21})^2 + (B_{S22})^2 + (B_{S23})^2} \tag{12}$$

Finally, using (13), the magnetic flux emitted by the conductors and detected by the sensor S_3 is computed.

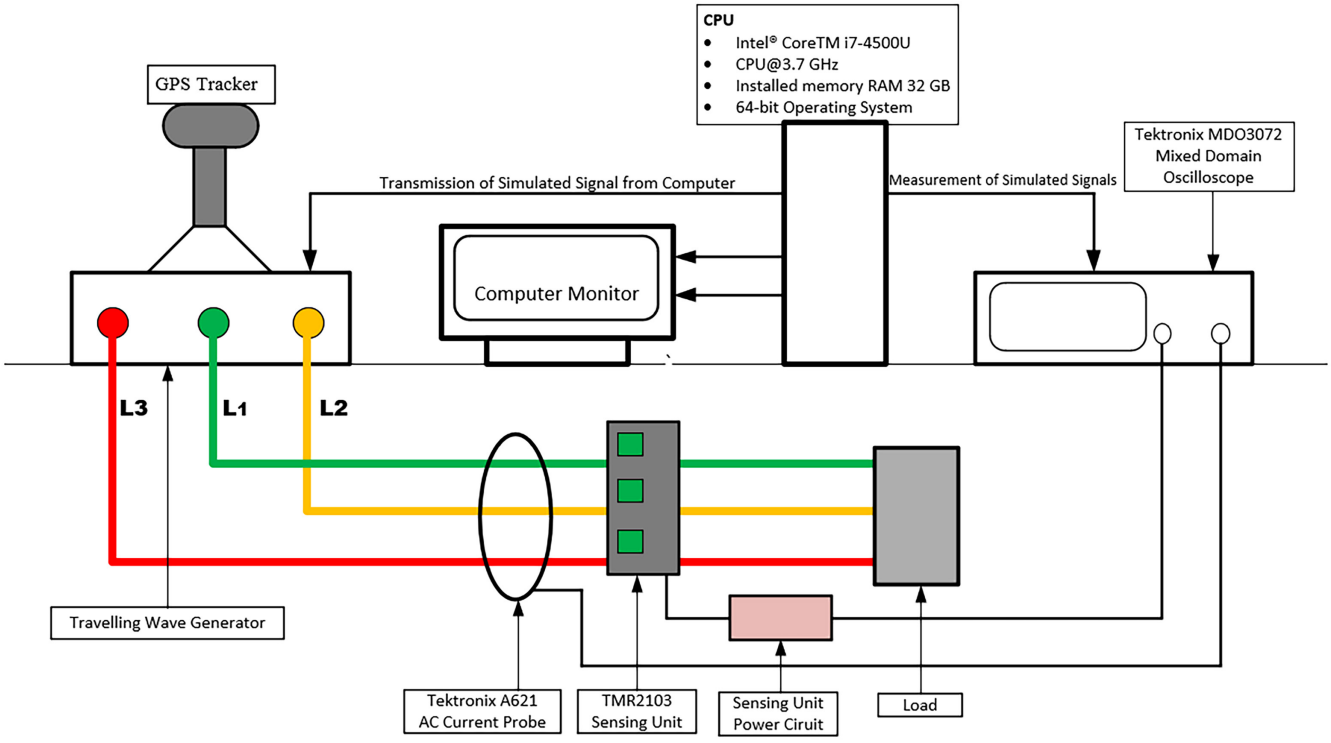

Fig. 5. Experimental set-up arrangement.

$$\begin{cases} B_{S31}(x,t)=\dfrac{\mu_0 I_{f1}(t)}{\pi L_{31}}\left((y_0-y_K)\sin\theta_{11}+(x_0-x_A)\cos\theta_{31}\right) \\ B_{S32}(x,t)=\dfrac{\mu_0 I_{f2}(t)}{\pi L_{32}}\left((y_0-y_Q)\sin\theta_{12}+(x_0-x_A)\cos\theta_{32}\right) \\ B_{S33}(x,t)=\dfrac{\mu_0 I_{f3}(t)}{\pi L_{33}}\left((y_0-y_K)\sin\theta_{33}+(x_0-x_A)\cos\theta_{33}\right) \end{cases} \quad (13)$$

The signals detected by sensor S_3 can be estimated based on (14).

$$B_{S3}(t)=\sqrt{(B_{S31})^2+(B_{S32})^2+(B_{S33})^2} \quad (14)$$

From (12), (14), and (16), L_{11}, L_{12}, L_{13}, L_{21}, L_{23}, L_{31}, L_{32}, and L_{33} are defined using (15).

$$\begin{cases} L_{11}=L_{33}=\sqrt{(x_0-x_A)^2+(y_0-y_K)^2} \\ L_{12}=L_{32}=\sqrt{(x_0-x_A)^2+(y_0-y_Q)^2} \\ L_{13}=L_{31}=\sqrt{\left(\dfrac{d}{2}\right)^2+(x_0-x_A)^2+(y_0-y_K)^2} \\ L_{21}=L_{23}=\sqrt{(x_0-x_A)^2+(h-y_Q)^2} \\ L_{22}=\sqrt{(x_0-x_A)^2+(h-y_Q)^2} \end{cases} \quad (15)$$

where d and h refer to the length and breadth of the array.

TABLE I.
OVERHEAD POWER LINE PARAMETERS

Voltage (kV)		**161**	**Line length (km)**		**200**
Short-Circuit Level at Tower A (MVA)		45	Short-Circuit Level at Tower B (MVA)		35
Positive	R_{pos} (Ω/km)	0.12	Zero	R_{zero} (Ω/km)	0.15
Sequence	L_{pos} (mH/km)	0.25	Sequence	L_{zero} (mH/km)	0.26
Parameters	R_{pos} (μ/km)	0.01	Parameters	C_{zero} (μ/km)	0.50

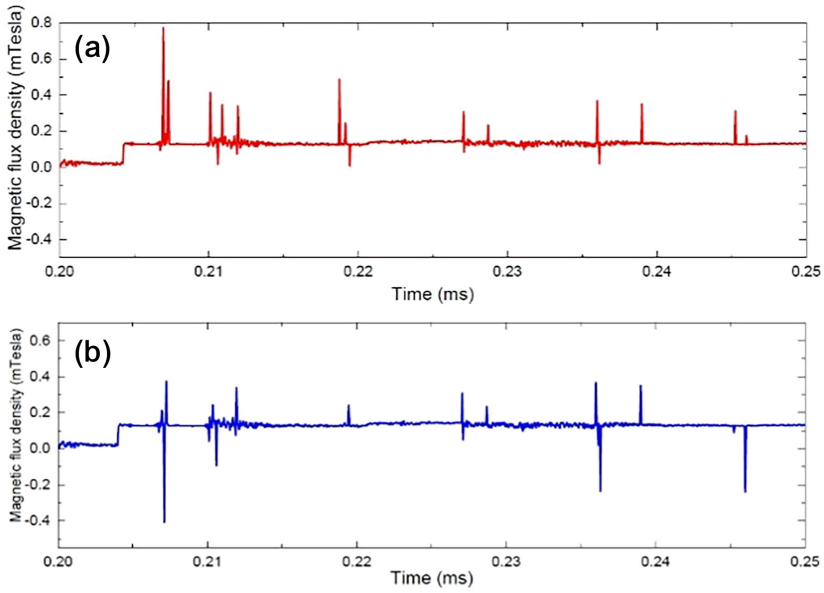

Fig. 6. (a) Flux density detected at tower T_A. (b) Flux density detected at tower T_B.

III. RESULTS

A. Laboratory Experiment

A laboratory test conducted to validate the proposed strategy is presented in this section of the paper, as shown in Fig. 5. Two simulation software programs were deployed in this study. The transmission line was modeled using MATLAB/Simulink, and the data were extracted and used in the Electrical Transient Analyzer Program (ETAP) for the entire analysis for the creation of transmission.

The transmission line under study is a 200 km line that has been modeled in MATLAB/Simulink using the parameters of transmission line parameters presented in Table I. The data obtained from the model were fed into a computer housing the ETAP software and interfaced with the traveling wave generator. From the ETAP model, a fault current traveling wave is created and fed into the traveling wave generator for analysis.

As seen in Fig. 5, an AC probe is then used to measure the current traveling waves. To estimate the flux based on (10), (12), and (14), the current traveling waves that were detected by the AC probe are fed into (9), (11), and (13). The sensors measure the flux densities produced by the traveling waves using (10), (12), and (14). The magnetic flux obtained is calculated based on (15). Fig. 6(a) and 6(b)

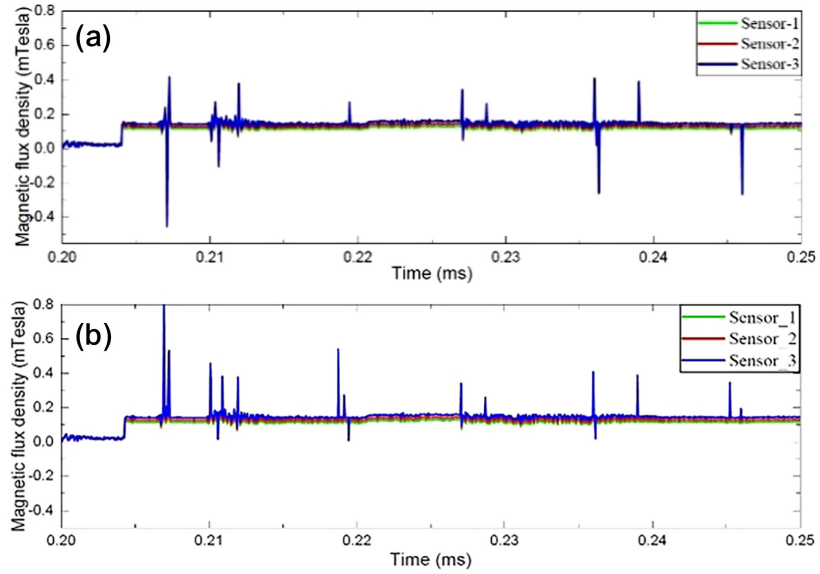

Fig. 7. Flux density measured by individual sensors at towers T_A and T_B.

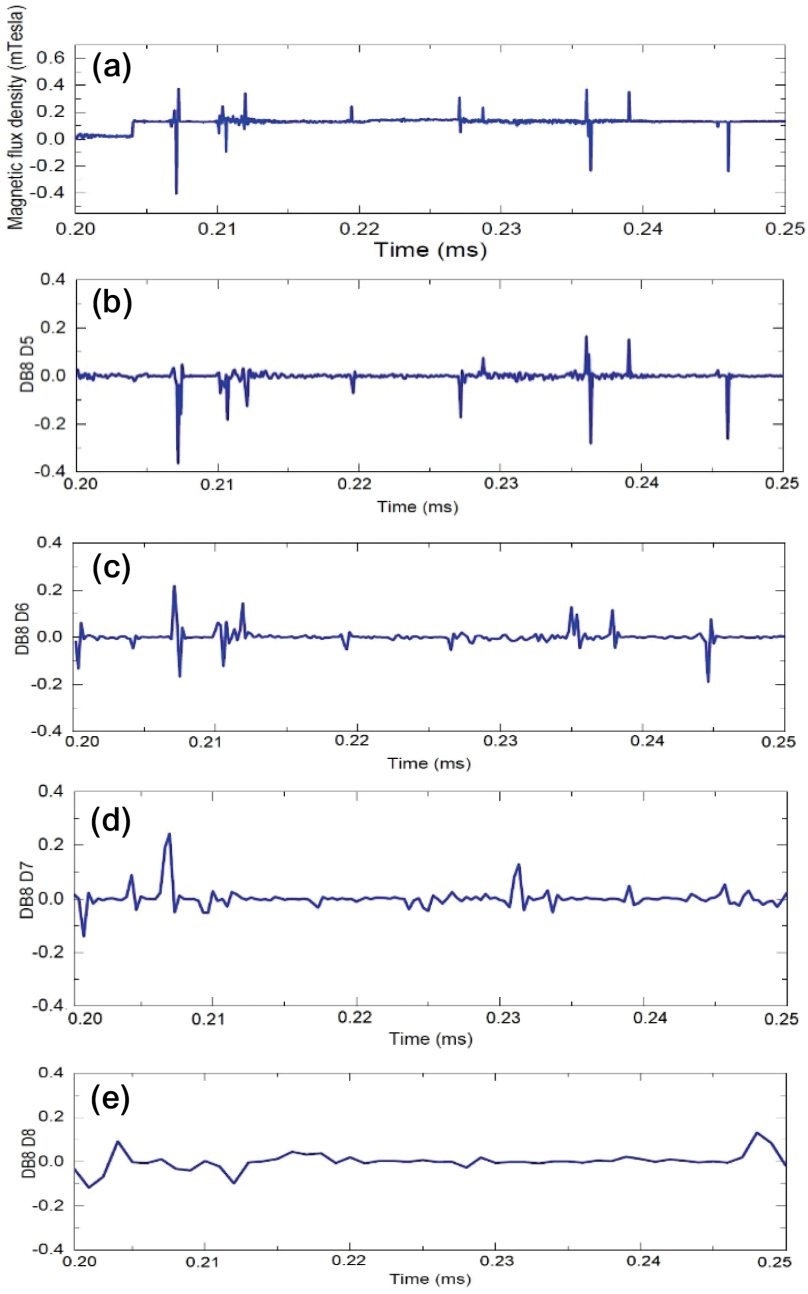

Fig. 8. Detailed coefficients of DB8 mother wavelet. (a) Flux density measured by the array. (b)–(e) Detailed wavelet coefficients of levels 5–8.

show the magnetic flux recorded at towers T_A and T_B respectively during an LLLG fault 75 km from both endpoints. Fig. 7 shows the performance of each individual sensor. The GPS tracker was used to timestamp the flux densities that were measured.

B. Wavelet Transforms Analysis of Signals for Fault Detection

A wavelet analysis of the magnetic flux produced by the traveling waves is performed to validate the proposed scheme. The wavelet transform coefficients are compared to the flux density or sensor array output. Due to its exceptional ability to extract signal information, experiments with various wavelets showed that Daubechies (DB8) was the best for this study. For the sensor output shown in Fig. 7, the DB8 restructuring of the coefficients at Daubechies (D5–D8) is shown in Fig. 8(b)–8(e). According to this waveform, the wave head is captured by the exact wavelet coefficients of levels 5 and 7. Above level 7, the detailed coefficients only display the output's low-frequency fluctuations.

C. Determining the Arrival Time of Traveling Waves

When employing the double-ended approach, as illustrated in (16), to locate faults in overhead power lines, the line length, the speed of the traveling waves, and the wave signal arrival time are considered.

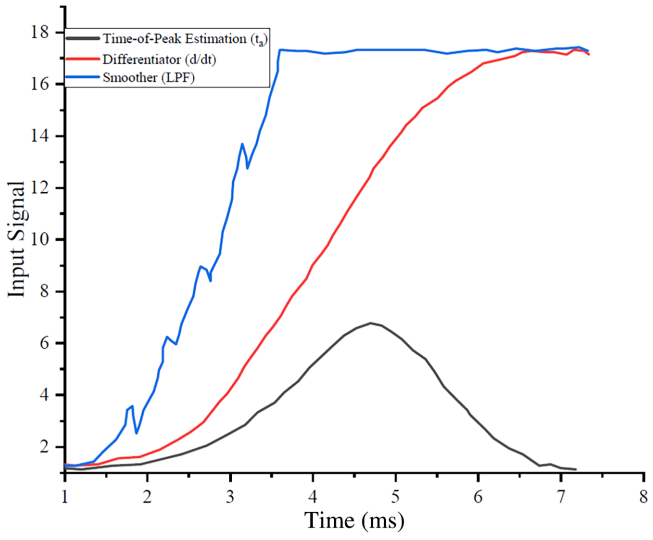

Fig. 9. Derivative of the input to the differentiator.

In this study, the transmission velocity of the traveling wave was based on the line length and the wave's traveling time. The traveling time was computed using the traveling wave data that the sensor array captured while the line was powered.

$$D_m = \frac{L}{2} - v\left(\frac{\cdot t_A + \cdot t_B}{2}\right) \tag{16}$$

where D_m is the measured fault distance, δt_A and δt_B are the difference in signal time of arrival (TOA) at towers T_A and T_B respectively.

Noise may alter the wave's TOA, leading to location mistakes when utilizing the non-contact current traveling wave technique to locate a transmission line fault point.

Three stages of signal processing were used to handle the flux density to lower the TOA estimation inaccuracy. The recorded signals are processed for noise removal and distortion reduction, and to preserve the high-frequency components of the original signal produced by the fault while discarding the system frequency components.

As seen in [11], the smoothed signals' output is routed into a differentiator. The wavefront's arrival time is less influenced by signal distortion since distinct signals provide a cleaner wavefront and peaks. Fig. 9 displays the derivative of the input of the three-stage signal processing.

D. Approximated Fault Distance and Error Analysis

Based on the experiment's findings, (16) is used to locate the fault point, and the differentiator smoother is used to predict when the current traveling wave signals would arrive. Based on (17), the relative error is calculated for every scenario.

$$\varepsilon\% = \frac{D_m - D_t}{L} * 100 \tag{17}$$

where D_m is the measured distance, D_t is the true distance, and L is the line length.

To validate the scheme proposed in this study, three different fault categories were considered: Line-to-ground (LG) fault, line-to-line-to-ground (LLG) fault, and line-to-line-to-line-to-ground (LLLG) fault, based on four different fault distances: 1 km, 34 km, 100 km, and 199 km.

TABLE II.
COMPARISON OF THE PROPOSED SCHEME FOR FAULT DISTANCE APPROXIMATION AND A GENERAL TRAVELING WAVE-BASED SCHEME

		A General Traveling Wave-Based Scheme [11]		Proposed Scheme	
Fault Category	**Actual Distance (km)**	**Approximated Fault Distance (km)**	**Approximated Error (%)**	**Approximated Fault Distance (km)**	**Approximated Error (%)**
Line-to-ground (LG)	1	0.93	0.035	0.97	0.015
	34	33.86	0.070	34.02	0.010
	100	100.0	0	100.10	0.050
	199	198.82	0.090	198.94	0.015
Line-to-line-to-ground (LLG)	1	0.93	0.035	0.97	0.015
	34	33.86	0.070	34.02	0.010
	100	100.0	0	100.10	0.050
	199	198.82	0.090	198.94	0.015
Line-to-line-to-line-to-ground (LLLG)	1	0.93	0.035	0.97	0.015
	34	33.86	0.070	34.02	0.010
	100	100.0	0	100.10	0.050
	199	198.82	0.090	198.94	0.015

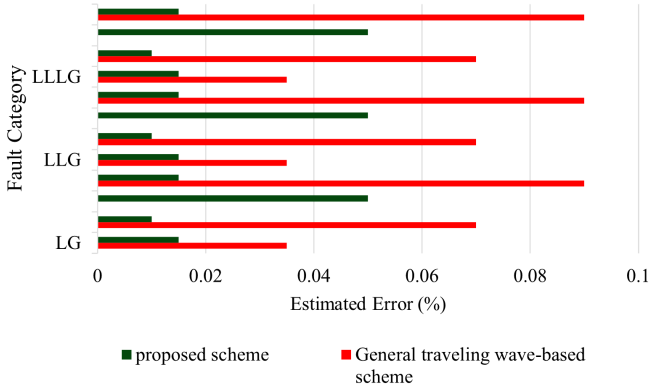

Fig. 10. Percentage error of the general traveling wave-based scheme against the proposed scheme.

The test cases considered include: 1 km, 34 km, 100 km, and 199 km all measured from tower T_A. The findings in Table II show that, in many situations, the proposed approach outperformed the general traveling wave-based method proposed in [11].

For each test case in this comparison, the differentiator smoother technique was employed to calculate the traveling wave arrival time. The proposed scheme had an average percentage error of 0.02445% for all fault categories in all test cases, whereas the generalized traveling wave-based method described in [11] had an average percentage error of 0.04842% for all fault kinds. Fig. 10 shows the relative mistakes between the two systems.

IV. CONCLUSION

This paper presents an innovative magnetic sensor-based traveling wave fault location scheme for overhead lines. To compute the fault point, the magnetic flux detected by the array is evaluated to determine the TOA and fault location. This work used the conventional wavelet transform combined with the smoother-based differentiator to compute the traveling wave arrival time. The outcome of the experiment validates the effectiveness of the proposed method for detecting and locating faults. The validity of the scheme is established by comparing it with a general traveling wave-based approach proposed in [11]. This proposal has the potential to significantly change the operation of modern power systems. Utility companies can drastically reduce outage durations, equipment damage, and service interruptions by adopting these fast fault detection and localization systems. The non-invasive nature of magnetic sensing improves safety and dependability while making installation and maintenance easier. Furthermore, the scalability of this strategy is consistent with the growth of the transmission network and the advancement of smart grid technology.

This proposed approach helps achieve sustainability, robustness, and an intelligent power system, which leads to a reduction in downtime, increased monitoring capabilities, and improved fault response. The adoption of this approach adoption is a promising step toward more robust and efficient energy transmission systems that address both current and future demands.

Availability of Data and Materials: The data that support the findings of this study are available upon request from the corresponding author.

Peer-review: Externally peer-reviewed.

Acknowledgments: The author would like to declare that the support of Anastasia Amissah, a BSc. Electrical and Electronics Engineering student of the Department of Electrical and Electronics Engineering at AAMUSTED, for proofreading the manuscript is greatly appreciated.

Author Contributions: Concept – P.N.A.; Design – P.N.A.; Supervision – P.N.A.; Resources – P.N.A.; Materials – P.N.A.; Data Collection and/or Processing – P.N.A.; Analysis and/or Interpretation – P.N.A.; Literature Search – P.N.A.; Writing – P.N.A.; Critical Review – P.N.A.

Declaration of Interests: The author has no conflicts of interest to declare.

Funding: This study received no funding.

REFERENCES

1. G. Wang, C. Zhuang, J. Deng, and Z. Xie, "A fault location method based on electromagnetic transient convolution considering frequency-dependent parameters and lossy ground," *IEEE Trans. Power Deliv.*, vol. 39, no. 2, pp. 1012–1022, 2024. [CrossRef]
2. X. Zhu, S. Li, Y. Guo, X. Chen, C. He, and J. Deng, "Novel wavefront detection and fault location method based on Hilbert-Huang transform for long HVDC transmission lines," *Electr. Power Syst. Res.*, vol. 211, pp. 108213. 2022. [CrossRef]
3. J. P. Triveno, V. P. Dardengo, and M. C. De Almeida, "An approach to fault location in HVDC lines using mathematical morphology," in *IEEE Power Energy Soc. Gen. Meet.*, (pp.1-5) 2015. [CrossRef]
4. S. Imai, D. Novosel, D. Karlsson, and A. Apostolov, "Unexpected consequences: Global blackout experiences and preventive solutions," *IEEE Power Energy Mag.*, vol. 21, no. 3, pp. 16–29, 2023. [CrossRef]
5. M. Bindi, M. C. Piccirilli, A. Luchetta, and F. Grasso, "A comprehensive review of fault diagnosis and prognosis techniques in high voltage and medium voltage electrical power lines," *Energies*, vol. 16, pp. 21, 2023. [CrossRef]
6. Y. Honcharov, N. Kriukova, V. Markov, and I. Poliakov, "Modern approaches of high-voltage transmission lines monitoring," *Bulletin of NTU "KhPI", Theor. Pract.*, vol. 2, no. 8, pp. 47–50, 2022. [CrossRef]
7. P. O. K. Anane, Q. Huang, O. Bamisile, and P. N. Ayimbire, "Fault location in overhead transmission line: A novel non-contact measurement approach for traveling wave-based scheme," *Int. J. Electr. Power Energy Syst.*, vol. 133, pp. 107233, 2021. [CrossRef]
8. P. N. Ayambire, Q. Huang, D. Cai, O. Bamisile, and P. O. K. Anane, "Real-time and contactless initial current traveling wave measurement for overhead transmission line fault detection based on tunnel magnetoresistive sensors," *Electr. Power Syst. Res.*, vol. 187, pp. 106508, 2020. [CrossRef]
9. P. C. Fernandes, H. N. G. Venzi Gonçalves, K. Melo E Silva, and F. Vigolvino Lopes, "Two-terminal modal traveling wave-based fault location method for HVDC systems," in *WCNPS*. 2018, pp. 1–4. [CrossRef]
10. D. Selvaratnam, A. Das, and H. Sandberg, "Electrical fault localisation over a distributed parameter transmission line," in *Proceedings of the IEEE Conference on Decision and Control*. 2023, pp. 7088–7093. [CrossRef]
11. H. A. Abd El-Ghany, A. M. Azmy, and A. M. Abeid, "A general travelling-wave-based scheme for locating simultaneous faults in transmission lines," *IEEE Trans. Power Deliv.*, vol. 35, no. 1, pp. 130–139, 2020. [CrossRef]

12. E. Personal, A. García, A. Parejo, D. Larios, F. Biscarri, and C. León, "A Comparison of Impedance-Based Fault Location Methods for Power Underground Distribution Systems," *Energies*, vol. 9, no. 12, pp. 1022, 2016. [CrossRef]
13. A. Bahmanyar, S. Jamali, A. Estebsari, and E. Bompard, "A comparison framework for distribution system outage and fault location methods," *Electric Power Systems Research*, vol. 145, pp. 19–34, 2017. [CrossRef]
14. S. S. Gururajapathy, H. Mokhlis, and H. A. Illias, "Fault location and detection techniques in power distribution systems with distributed generation: A review," *Renewable and Sustainable Energy Reviews*, vol. 74, pp. 949–958, 2017. [CrossRef]
15. E. O. Schweitzer, A. Guzman, M. V. Mynam, V. Skendzic, B. Kasztenny, and S. Marx, "Protective relays with traveling wave technology revolutionize fault locating," *IEEE Power Energy Mag.*, vol. 14, no. 2, pp. 114–120, 2016. [CrossRef]
16. H. Panahi, R. Zamani, M. Sanaye-Pasand, and H. Mehrjerdi, "Advances in transmission network fault location in modern power systems: Review, outlook and future works," *IEEE Access*, vol. 9, pp. 158599–158615, 2021. [CrossRef]
17. H. Jia, "An improved traveling-wave-based fault location method with compensating the dispersion effect of traveling wave in wavelet domain," *Math. Probl. Eng.*, vol. 2017, no. 1, pp. 1019591, 2017. [CrossRef]
18. R. J. Hamidi, and H. Livani, "Traveling-wave-based fault-location algorithm for hybrid multiterminal circuits," *IEEE Trans. Power Deliv.*, vol. 32, no. 1, pp. 135–144, 2017. [CrossRef]
19. M. Majidi, M. Etezadi-Amoli, and M. S. Fadali, "A sparse-data-driven approach for fault location in transmission networks," *IEEE Trans. Smart Grid*, vol. 8, no. 2, pp. 1–9, 2015. [CrossRef]
20. C. Subramani, A. A. Jimoh, M. M. Sudheesh, and I. E. Davidson, "Fault investigation methods on power transmission line: A comparative study," in IEEE PES PowerAfrica Conference, PowerAfrica 2016, pp. 93-97, 2016. [CrossRef]
21. M. Cervantes, I. Kocar, J. Mahseredjian, and A. Ramirez, *A Traveling Wave Based Fault Location Method Using Unsynchronized Current Measurements*, pp. 1-1, 2020. [CrossRef]
22. O. Naidu, and A. K. Pradhan, "A traveling wave-based fault location method using unsynchronized current measurements," *IEEE Trans. Power Deliv.*, vol. 34, no. 2, pp. 505–513, 2019. [CrossRef]
23. M. Fayazi, M. Joorabian, A. Saffarian, and M. Monadi, "A single-ended traveling wave based fault location method using DWT in hybrid parallel HVAC/HVDC overhead transmission lines on the same tower," *Electr. Power Syst. Res.*, vol. 220, pp. 109302, 2023. [CrossRef]
24. M. Duan, Y. Liu, D. Lu, and R. Pan, "A novel noniterative single-ended fault location method with distributed parameter model for AC transmission lines," *Int. J. Electr. Power Energy Syst.*, vol. 153, pp. 109358, 2023. [CrossRef]
25. Y. Wang, T. Zheng, C. Yang, and L. Yu, "Traveling-wave based fault location for phase-to-ground fault in non-effectively earthed distribution networks," *Energies*, vol. 13, no. 19, pp. 5028, 2020. [CrossRef]
26. P. N. Ayambire, H. Qi, P. O. K. Anane, A. K. Awopone, L. Jian, and O. Bamisile, "An Improved Fault Detection Method for Overhead Transmission Lines Based on Differential Tunnel Magnetoresistive Sensor Array Approach," *IEEE Can. J. Electr. Comput. Eng.*, vol. 45, no. 4, pp. 409–417, 2022. [CrossRef]
27. N. M. Belčević, and Z. N. Stojanović, "Using voltage signals for transient fault detection on overhead lines," *Int. J. Electr. Power Energy Syst.*, vol. 137, pp. 107824, 2022. [CrossRef]
28. J. Reymond, A. Serway, and J. W. Jewett, *Modern Physics for Scientists and Engineers*, pp. 911, 2014.